Taylor-Fourier PMU on a Real-Time Simulator: Design, Implementation and Characterization

G. Frigo*, A. Derviškadić*, Y. Zuo*, A. Bach†, M. Paolone*
*École Polytechnique Fédérale de Lausanne, 1015 Lausanne, Switzerland
†École Normale Supérieure de Cachan, Université Paris-Saclay, Paris, France
mail: {guglielmo.frigo, asja.derviskadic}@epfl.ch

***Abstract*—The development of software models of Phasor Measurement Units (PMUs) within Real-Time Simulators (RTSs) represents a promising tool for the design and validation of monitoring and control applications in electrical power networks. In this sense, it is necessary to find an optimal trade-off between computational complexity and estimation accuracy. In this paper, we present the design and implementation of two new PMU models within the Opal-RT eMEGAsim RTS. The synchrophasor estimation algorithm relies on a Compressive Sensing Taylor-Fourier Model (CS-TFM) approach, and enables us to extract the dynamic phasor associated to the signal fundamental component. The estimation accuracy of the proposed models is characterized with respect to the compliance tests of the IEEE Std. C37.118.1.**

***Index Terms*—Real-Time Simulator (RTS), Synchrophasor, Taylor-Fourier Transform, Phasor Measurement Unit (PMU)**

I. Introduction

In recent years, Phasor Measurement Units (PMUs) have become an effective and reliable solution for the monitoring and control of electrical power networks [1], [2]. In this context, the IEEE Std C37.118.1 [3] and its recent amendment [4] (briefly IEEE Std) define PMUs as high-accuracy devices for synchronized phasor and frequency measurements. In particular, PMUs are required to characterize the fundamental tone in terms of phasor amplitude and phase, frequency, and Rate-of-Change-of-Frequency (ROCOF). Furthermore, PMU measurements are phase-aligned to a common time-reference synchronized with Universal Time Coordinates (UTC).

Before the actual deployment into the field, PMUs have to be thoroughly validated and characterized in terms of estimation accuracy and reporting latency with respect to both IEEE Std tests and expected operating conditions. Also, before their deployment into real power networks, PMU-based control and protection schemes have to be validated in terms of reliability and effectiveness. Since an experimental validation might be partially uncontrollable or even unfeasible, the employment of a Real Time Simulator (RTS) enables us to reproduce a wide range of realistic operating conditions and therefore evaluate the reliability of PMU-based applications even during critical scenarios [5], [6]. In this context, the development of PMU software models might become a promising solution as they allow for reproducing large-scale applications involving multiple PMUs.

Once defined the electrical network under investigation, the RTS reproduces the system behavior in terms of nodal voltages and currents. In this context, the integration of PMUs can be carried out according to two alternative options.

In the first option, the RTS is interfaced with real PMUs by means of analog output channels, capable of reproducing power signals. Through a Local Access Network (LAN), PMUs are connected to a Phasor Data Concentrator (PDC) that collects the measurement data and aligns them based on the corresponding time-stamp [7]. This option enables us to test the actual device (not limited to the synchrophasor extraction algorithm) and to reduce significantly the complexity of the RTS model. However, this approach is characterized by several drawbacks: (i) the uncertainty characterization of the RTS power signals, (ii) the limited number of available analog output channels, (iii) the cost of real PMUs, (iv) the amount of cabling. Due to these limitations, this solution cannot support large-scale network models.

In the second option, instead, the PMUs are simulated and included within the RTS model. In this way, the validation process is independent from the device and accounts also for the transfer function of the instrument transformers. It is possible to reproduce large-scale networks and validate monitoring and control applications relying on numerous (e.g. hundreds) PMUs. The only limitation is represented by the computational resources of the RTS. As a consequence, the complexity of the PMU model should be possibly reduced, in order to find an optimal trade-off between estimation accuracy and computational requirements [8].

Inspired by a similar analysis in [8], in this paper, we present the design, implementation and characterization of two new PMU models within the Opal-RT eMEGAsim RTS [9]. In particular, we adopt a synchrophasor estimation algorithm, that has been derived by the recent Compressive Sensing Taylor-Fourier Model (CS-TFM) [10]. To the best of Authors' knowledge, this represents the first attempt to implement a PMU model relying on a dynamic phasor formulation [11] and thus capable of tracking the signal time-variations and directly computing ROCOF as one of the system state variables.

The RTS results rely on the assumption that PMU models are characterized by the same accuracy and responsiveness of the actually deployed devices. For this reason, we evaluate its estimation accuracy in terms of Total Vector Error (TVE), Frequency Error (FE) and ROCOF Error (RFE), and we assess its computational complexity in terms of maximum number of PMUs per RTS core and computation time. For this analysis,

we consider the IEEE Std tests, with specific reference to the Protection and Measurement class requirements, referred to as P- and M-class respectively, as well as an off-standard test inspired by real-world operating conditions [12].

The paper is organized as follows. Section II introduces the algorithm theoretical background. Section III describes the implementation within the Opal-RT simulation environment. Section IV presents a thorough performance characterization. Finally, Section V provides closing remarks.

II. Theoretical Background

Let us consider a generic time-varying power signal, affected by both narrow- and wide-band disturbances:

$$x(t) = A \cdot (1 + \varepsilon_A(t)) \cdot \cos(2\pi f t + \varphi + \varepsilon_\varphi(t)) + \eta + \rho \quad (1)$$

where A, f and φ are the amplitude, frequency and initial phase of the fundamental component, respectively. The time-varying terms ε_A and ε_φ account for amplitude and phase modulations, η represents any spurious component, and ρ models the measurement uncertainty as an additive uncorrelated Gaussian random variable.

Typically, a PMU considers an observation window of finite length N_w and computes its Discrete Fourier Transform (DFT) $X(f)$ in order to extract the synchrophasor associated to the fundamental component [13]. However, the DFT-based approach relies on a static signal model and cannot provide an optimal representation of dynamic conditions. For this reason, the recent literature has discussed the employment of Taylor series expansions, whose higher-order derivative terms might better account for fundamental time-varying parameters [11].

In this context, the CS-TFM algorithm adopts a formulation of the Taylor-Fourier Transform (TFT) [14], that has been suitably modified and generalized in order to deal also with multi-tone power signals. In its original formulation, the TFT has been presented as a maximally flat differentiator filter, centered around the nominal system frequency[1] [15]. Thanks to a Taylor series expansion truncated to the second derivative order, it is possible to include the fundamental frequency and ROCOF within the estimator state variables as the first and second time-derivative of the phase angle, respectively. However, the TFT performance strongly depends on the spectral support $\mathcal{S}$ employed for the filter positioning [16]: if any significant spectral component is neglected or badly identified, the TFT results might suffer from uncompensated spectral leakage and thus lead to inaccurate estimates [17].

For this reason, the identification of the signal spectral support $\mathcal{S}$ becomes one of the most crucial stages of the entire synchrophasor extraction algorithm. On the other hand, the processing resources destined to $\mathcal{S}$ identification should comply with the capabilities of the selected implementation platform. Recent literature has proposed to track the fundamental frequency by means of a Phase Locked Loop (PLL) algorithm [18] or a Kalman Filter (KF) [19]. Similar solutions, though, are prone to errors since they rely on the unverified assumption that the fundamental frequency is slowly varying between two consecutive observation windows. In the presence of sudden parameter changes, PLL and KF introduce a filtering effect (with delayed and smoothed transitions) that might result in a significant accuracy degradation [20].

In this paper, as in [10], we recover the spectral support $\mathcal{S}$ through an Orthogonal Matching Pursuit (OMP) algorithm, i.e. a *greedy* selection routine that exploits the assumption that the signal spectrum is sparse and consists only of a limited number of narrow-band components. In particular, we apply a CS-based super-resolution technique to improve the frequency resolution associated to short observation intervals by almost one order of magnitude (further details in [21]).

Given the recovered support $\mathcal{S}$, we design the corresponding TFM model M and we compute the dynamic synchrophasor p that consists of three Taylor-Fourier series coefficients:

$$p = \{p^0, p^1, p^2\} = \text{pinv}(M) \cdot x \quad (2)$$

where the superscript denotes the derivative order. Based on this, we are able to estimate the fundamental parameters as:

$$\begin{aligned} \hat{A} &= |p^0|, & \hat{A}^1 &= 2\Re(p^1 \cdot e^{-j\hat{\varphi}}) \\ \hat{\varphi} &= \angle p^0, & \varphi^1 &= \frac{\Im(p^1 \cdot e^{-j\hat{\varphi}})}{\hat{A}} \\ \hat{f} &= \hat{f}_0 + \frac{\hat{\varphi}^1}{2\pi}, & \hat{R}_f &= \frac{\Im(p^2 \cdot e^{-j\hat{\varphi}}) - \hat{A}^1 \cdot \hat{\varphi}^1}{2\pi \cdot \hat{A}} \end{aligned} \quad (3)$$

where $\hat{R}_f$ denotes the ROCOF, and f_0 is the fundamental frequency within the recovered spectral support.

A. Modulated Sliding DFT

In terms of measurement reporting latency, the DFT computation requires a significant amount of processing time, as its complexity $\mathcal{O}(N_w^2)$ can be reduced up to $\mathcal{O}(N_w \log N_w)$ with the Fast Fourier Transform algorithm [22]. Nevertheless, the synchrophasor analysis does not consider the entire spectrum, but focuses on a narrow bandwidth centered around the nominal system frequency. Therefore, it is possible to limit the number of DFT bins to be computed. In particular, the proposed algorithm restricts its analysis up to the out-of-band (OOB) frequency range, i.e. from 5 to 100 Hz (see Sec. II.B)[2].

In this context, an effective solution for the DFT bins' computation is represented by the Modulated Sliding DFT (MSDFT) algorithm [24], a recursive routine for computing DFT bins on a sample-by-sample basis. In order to resolve multiple spectral tones, we apply a Hanning weighing function through a frequency-domain convolution that results in a linear combination of adjacent DFT bin values:

$$X_k = -0.25 \cdot X_{k-1} + 0.5 \cdot X_k - 0.25 \cdot X_{k+1} \quad (4)$$

[1]Without loss of generality, in this paper we consider a nominal system frequency of 50 Hz, but similar results can be obtained in a 60-Hz scenario.

[2]Given a system frequency of 50 Hz, we adopt the inter-harmonic group formulation as defined in [23]. Nevertheless, according to IEEE Std, PMUs should not consider the DC component, and the lowest sub-harmonic group is typically centered around 5 Hz.

where the subscript k denotes the bin index. In this way, we are able to significantly reduce the computational effort as well as to guarantee the DFT stability and accuracy [25], [26].

B. Taylor-Fourier Model Algorithm

As known, the IEEE Std introduces two PMU performance classes: the P-class is intended for protection applications and favors fast responsiveness rather than high accuracy, conversely M-class is intended for measurement applications and requires high accuracy also in distorted conditions [3].

In order to cope with these contrasting requirements, we develop two models specifically designed for P- and M-class compliance, whose main processing steps are reported in Algorithm 1 and 2, respectively.

a) P-class Model: The P-class PMU adopts a window length of 60 ms, i.e. equal to three nominal cycles at 50 Hz and corresponding to a frequency resolution of 16.67 Hz.

In P-class configuration, we are not interested in detecting and compensating possible inter-harmonic components. The spectral analysis can be limited to the expected variation range of the fundamental component, i.e. [45, 55] Hz. To this end, the MSDFT provides a DFT representation X consisting of just 3 bins, centered at 33.33, 50 and 66.67 Hz, respectively.

As shown in Algorithm 1, the first step consists in enhancing the frequency resolution by projecting X over the vector space spanned by matrix D_f. In more detail, the matrix columns are designed to account for leakage effects over a super-resolved grid, whose bin spacing is set to 1.515 Hz (line 3).

We associate the fundamental frequency $\hat{f}_0$ to the maximum bin of the super-resolved spectrum (line 4), and we include into the spectral support $\mathcal{S}$ the first four harmonic terms (line 5). Based on this information, we construct the TFM matrix (line 6) and compute the corresponding dynamic phasor coefficients (line 7). Finally, by applying (3), we extract the fundamental synchrophasor, frequency and ROCOF (line 8).

Algorithm 1 P-class Model

1: **P-class** $\rightarrow$ window length 60 ms, 3 DFT bins
2: *input:* x, X, D_f, *output:* $\hat{A}, \hat{f}, \hat{\varphi}, \hat{R}_f$
3: $Y = D_f^{\dagger} \cdot X$ ▷ super-resolved spectrum
4: $\hat{f}_0 = \max(Y)$ ▷ fund. frequency estimate
5: $\mathcal{S} = \{\hat{f}_0 \cdot [1, 2, 3, 4]\}$ ▷ spectral support definition
6: $M = TFM(\mathcal{S})$ ▷ TFM matrix computation
7: $p = (M^{\dagger}M)^{-1}M^{\dagger} \cdot x$ ▷ dynamic phasor extraction
8: $\hat{f}_0, p \rightarrow \{\hat{A}, \hat{f}, \hat{\varphi}, \hat{R}_f\}$ ▷ final parameter estimates

b) M-class Model: Differently from P-class scenario, M-class PMUs are intended for higher accuracy and robustness in the presence of harmonic and out-of-band disturbances, even if this means larger response time and reporting latency. To this end, the M-class model adopts a window length of 100 ms, i.e., equal to five nominal cycles at 50 Hz and corresponding to a frequency resolution of 5 Hz.

In order to mitigate the leakage effects due to spurious components, we need to identify their frequency and include it into the spectral support $\mathcal{S}$. For this reason, the MSDFT computes 14 bins as representative of the fundamental variation range [45, 55] Hz and the out-of-band[3] frequency range [5, 25] $\cup$ [75, 95] Hz. As shown in Algorithm 2, we first project the signal spectrum over a finer grid whose resolution is of 0.909 Hz (line 3). Then, we identify the fundamental component as the maximum spectral bin (line 4). Based on its amplitude, frequency and phase, we subtract its contribution from the original spectrum (line 5) and we apply the super-resolution routine over the OOB range (line 6).

Within the residual spectrum, we select the maximum bin (line 7): if its amplitude exceeds the significance threshold θ_i, the corresponding frequency is included in the spectral support, otherwise $\mathcal{S}$ accounts only for the first four harmonic terms (lines from 8 to 12). In concordance with the IEEE Std requirements for the *Out-of-Band interference* test, we set θ_i equal to five percent of fundamental amplitude. In practice, though, this parameter has to be set according to the desired sensitivity to spurious tones and the expected noise level, in order to avoid the inclusion of negligible components into $\mathcal{S}$.

Finally, based on the recovered spectral support, we construct the TFM matrix (line 13), we compute the dynamic phasor coefficients (line 14), and we extract the fundamental component parameters (line 15).

Algorithm 2 M-class Model

1: **M-class** $\rightarrow$ window length 100 ms, 11 DFT bins
2: *input:* x, X, D_f, D_i, θ_i, *output:* $\hat{A}, \hat{f}, \hat{\varphi}, \hat{R}_f$
3: $Y = D_f^{\dagger} \cdot X$ ▷ super-resolved spectrum
4: $(\hat{f}_0, \hat{A}_0, \hat{\varphi}_0) = \max(Y)$ ▷ fund. parameter estimates
5: $R = Y - \hat{A}_0 e^{j2(\pi \hat{f}_0 + \hat{\varphi}_0)}$ ▷ residual OOB spectrum
6: $Y = D_i^{\dagger} \cdot R$ ▷ super-resolved spectrum
7: $(\hat{f}_i, \hat{A}_i) = \max(Y)$ ▷ inter-harmonic selection
8: **if** $\hat{A}_i \geq \theta_i$
9: $\quad \mathcal{S} = \{\hat{f}_0 \cdot [1, 2, 3, 4], \hat{f}_i\}$ ▷ spectral support def.
10: **else**
11: $\quad \mathcal{S} = \{\hat{f}_0 \cdot [1, 2, 3, 4]\}$ ▷ spectral support def.
12: **end if**
13: $M = TFM(\mathcal{S})$ ▷ TFM matrix computation
14: $p = (M^{\dagger}M)^{-1}M^{\dagger} \cdot x$ ▷ dynamic phasor extraction
15: $\hat{f}_0, p \rightarrow \{\hat{A}, \hat{f}, \hat{\varphi}, \hat{R}_f\}$ ▷ final parameter estimates

III. Opal-RT Implementation

a) Real-Time Simulator (RTS): The development of a PMU model within a RTS requires the implementation of two main functionalities: the synchrophasor estimation algorithm, and the synchronization to a UTC-traceable time-source.

For this analysis, we employed the Opal-RT eMEGAsim PowerGrid Real-Time Digital Simulator [9], whose block scheme is presented in Fig. 1. In more detail, the RTS consists of three main operational blocks: an industrial PC with 12 cores, a Dolphin DXE410 PCI Express Expansion Chassis

[3]The IEEE Std defines the out-of-band frequency range based on the nominal system frequency and the adopted reporting rate. For this analysis, we set both these parameters equal to 50 Hz, as typical of M-class applications.

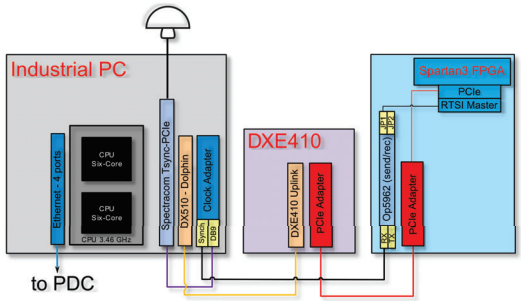

Fig. 1. Block scheme of the eMEGAsim PowerGrid RTS adapted from [8].

TABLE I
PMU MODELS' COMPUTATIONAL COMPLEXITY

PMU Model	PMUs per Core	Computation Time [μs]
P-class	5	16
M-class (no OOB)	2	42
M-class (with OOB)	1	56

[27], and a Spartan-3 Field Programmable Gate Array (FPGA) board [28]. The industrial PC runs the RTS model with an integration time-step of 100 μs, the FPGA board locks the internal time-base to a more stable clock, and the DXE410 module enables the communication between the other two blocks. In this regard, the alignment to UTC is provided by the Spectracom Tsync-PCIe Express board [29]. This hardware module employs a Global Positioning System (GPS) antenna to provide the UTC timestamp for the PMU data-frames, and the Pulse-per-Second (PPS) signal for the internal time-base.

b) Computational Complexity: The simulation of a large-scale PMU-based application depends on the adopted model complexity. In this sense, Table I reports the computational requirements of the P- and M-class models. For this analysis, we consider two performance indexes: the number of PMUs that we can include in a single RTS processing core, and the computation time given an integration time of 100 μs.

In the P-class configuration, the estimation process requires only 16 μs, corresponding to a maximum number of five PMUs in the same core. The M-class configuration, instead, involves a higher number of processing steps that results also in higher complexity. In this regard, we discriminate the contribution due to the OOB search and compensation. If we consider only the harmonic terms, the computation time is limited to 42 μs and we can include two PMUs in the same core. If we consider also possible OOB components, the computation time raises up to 56 μs and we can associate a single PMU to each core.

IV. PERFORMANCE CHARACTERIZATION

In this Section, we report the performance characterization of P- and M-class models with respect to the corresponding IEEE Std requirements[4] and in a real-world operating scenario.

[4]A thorough performance assessment of CS-TFM algorithm is available in [10] where also more realistic test conditions are taken into account.

For this analysis, we set the sampling frequency equal to 5 kHz, and we consider an overall test duration of 2 s (with the only exception of *Frequency ramp* test, whose duration is set equal to 4 and 10 s for P- and M-class, respectively). The PMU reporting rate is set equal to 50 fps. In order to model realistic measurement conditions, the test waveforms are intentionally corrupted by an uncorrelated Gaussian noise with a Signal-to-Noise Ratio (SNR) of 80 dB.

As performance indexes, we consider five metrics: Amplitude Error (AE), Phase Error (PE), Total Vector Error (TVE), Frequency Error (FE) and ROCOF Error (RFE). In this regard, Table II and III report the worst-case performance as function of test condition in P- and M-class, respectively, and compare them with the corresponding IEEE Std limits.

As regards P-class, it is worth noticing how the PMU model complies with the IEEE Std requirements in all the static and dynamic tests. In nominal steady-state conditions, the PMU model provides a worst-case TVE of 0.003%, whereas FE and RFE do not exceed 0.21 mHz and 0.03 Hz/s, respectively. As expected, the worst performance is obtained in the *Harmonic distortion* test. Indeed, the scarce frequency resolution (just 16.67 Hz) produces significant spectral leakage from harmonic terms, that results in a performance degradation, e.g. worst-case FE might achieve 3.88 mHz. Nevertheless, all the performance metrics comply with the IEEE Std requirements.

Similar considerations hold also for class-M compliance tests. In nominal steady-state conditions, the estimation accuracy is comparable with P-class results, thus confirming that the main limiting factor is represented by the measurement noise. The *Out-of-band interference* test proves that it is possible to mitigate distortion effects coming from inter-harmonic components, if properly included into the spectral support $\mathcal{S}$. Once more, the *Harmonic distortion* test provides the worst performance, with a TVE in the order of 0.2%, yet still complies with the IEEE Std limits.

Then, we study the models' behavior in the presence of transient events, like amplitude or phase step changes, when the signal energy is conveyed over the entire spectrum and the synchrophasor model looses its significance. In this case, the IEEE Std requires to determine the measurement response time, i.e. the time interval necessary for TVE and FE to return within the limits for steady-state test (TVE$\leq$1%, FE$\leq$5 mHz).

In this context, Fig. 2 and 3 represent the evolution of TVE and FE in the step tests for P- and M-class, respectively, whereas Table IV reports the measured response times and compares them with the IEEE Std limits. The compliance is guaranteed in all the configurations, with the only exception of the P-class response to *Phase step* test. In fact, the combination of Hanning weighing function and spectral energy spreading produces a fundamental main-lobe that can be hardly modeled by the super-resolution dictionary D_f [30]. As a consequence, the support recovery fails and the corresponding TFM model is not properly centered around the fundamental frequency, with a consequent degradation of the final estimation accuracy. In this sense, a plausible solution might be the employment of a narrower weighing window (e.g. Kaiser window) or a shorter

TABLE II
WORST-CASE ESTIMATION UNCERTAINTY FOR P-CLASS IEEE STD COMPLIANCE - THREE-CYCLE WINDOW

Test	AE [pu]	PE [rad]	TVE [%]	Std [%]	FE [mHz]	Std [mHz]	RFE [Hz/s]	Std [Hz/s]
nominal	$2.36{\cdot}10^{-5}$	$2.64{\cdot}10^{-5}$	0.003	1	0.208	5	0.027	0.4
signal freq. (f_0 = ±2 Hz)	$5.13{\cdot}10^{-5}$	$5.62{\cdot}10^{-5}$	0.007	1	3.378	5	0.089	0.4
harm. dist. (THD = 1%)	$3.56{\cdot}10^{-4}$	$4.19{\cdot}10^{-4}$	0.044	1	3.883	5	0.189	0.4
ampl. mod. (f_m = 2 Hz)	$4.99{\cdot}10^{-5}$	$4.32{\cdot}10^{-5}$	0.006	3	0.183	60	0.073	2.3
phase mod. (f_m = 2 Hz)	$3.69{\cdot}10^{-5}$	$5.37{\cdot}10^{-5}$	0.005	3	2.754	60	0.066	2.3
freq. ramp (Δ_f = ±2 Hz)	$2.16{\cdot}10^{-5}$	$3.27{\cdot}10^{-5}$	0.004	1	0.104	10	0.049	0.4

TABLE III
WORST-CASE ESTIMATION UNCERTAINTY FOR M-CLASS IEEE STD COMPLIANCE - FIVE-CYCLE WINDOW

Test	AE [pu]	PE [rad]	TVE [%]	Std [%]	FE [mHz]	Std [mHz]	RFE [Hz/s]	Std [Hz/s]
nominal	$2.67{\cdot}10^{-5}$	$5.85{\cdot}10^{-6}$	0.003	1	0.177	5	0.025	0.1
signal (f_0 = ±5 Hz)	$3.84{\cdot}10^{-5}$	$3.83{\cdot}10^{-5}$	0.004	1	0.261	5	0.037	0.1
harm. dist. (THD = 10%)	$1.59{\cdot}10^{-3}$	$1.84{\cdot}10^{-3}$	0.192	1	17.82	25	1.210	-
out-of-band (TIHD = 10%)	$1.73{\cdot}10^{-4}$	$1.98{\cdot}10^{-5}$	0.016	1.3	0.307	10	0.041	-
ampl. mod. (f_m = 5 Hz)	$4.12{\cdot}10^{-4}$	$7.66{\cdot}10^{-5}$	0.050	3	2.693	300	0.789	14
phase mod. (f_m = 5 Hz)	$4.18{\cdot}10^{-4}$	$4.28{\cdot}10^{-4}$	0.055	3	38.15	300	1.107	14
freq. ramp (Δ_f = ±5 Hz)	$2.69{\cdot}10^{-5}$	$3.11{\cdot}10^{-5}$	0.004	1	1.009	10	0.057	0.2

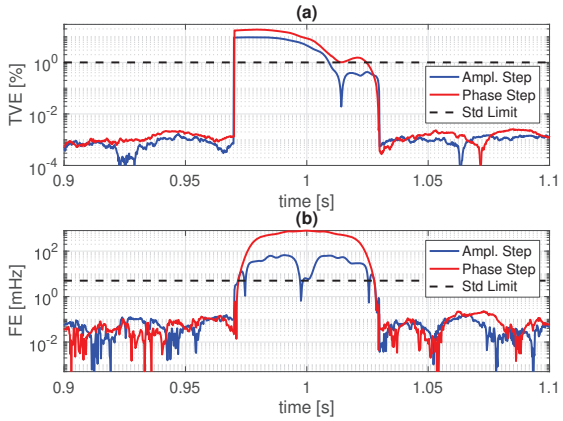

Fig. 2. Evaluation of measurement response times for P-class configuration in the *Amplitude step* and *Phase step* tests in blue and red line, respectively. The dashed black line represents the corresponding IEEE Std limit.

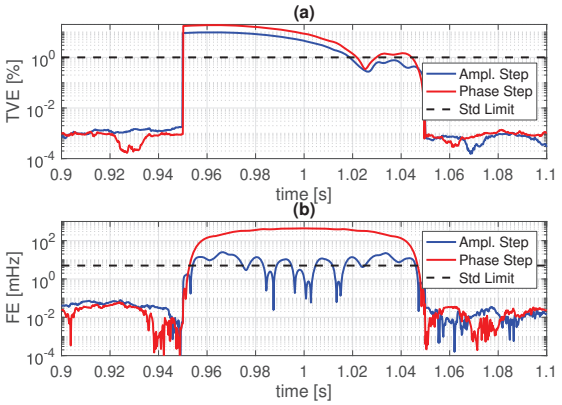

Fig. 3. Evaluation of measurement response times for M-class configuration in the *Amplitude step* and *Phase step* tests in blue and red line, respectively. The dashed black line represents the corresponding IEEE Std limit.

window length (e.g. 40 ms) [31], though it might result in a performance degradation in the other test conditions.

Finally, we evaluate the PMU models' performance by using a synthetic dataset inspired by a real-world network event. In particular, the test waveform derives from the recording of an inter-area oscillation of the Continental Europe electricity system recorded on December 1, 2016 (further details in [12]). As shown in Fig. 4(a) the fundamental frequency exhibits a time-varying trend characterized by superposed modulations and linear ramps. Even in such a challenging operating condition, both the PMU models prove to provide accurate estimates, keeping FE within ±200 and ±75 μrad for P- and M-class configuration, respectively.

TABLE IV
RESPONSE TIME IN IEEE STD STEP CHANGES TESTS

Model	Step	TVE	Std	FE	Std
P-class	Amplitude (±0.1 pu)	39.2	40	56.4	90
	Phase (±π/10 rad)	55	40	56.2	90
M-class	Amplitude (±0.1 pu)	69	140	92	280
	Phase (±π/10 rad)	94	140	94.4	280

V. CONCLUSIONS

In this paper, we presented the design, implementation and characterization of two TF-based PMU models within a RTS.

First, we discussed the theoretical background of the adopted synchrophasor extraction algorithm, i.e., CS-TFM. In this sense, we focused on the processing routines employed to compute the DFT bins and the TF expansion coefficients.

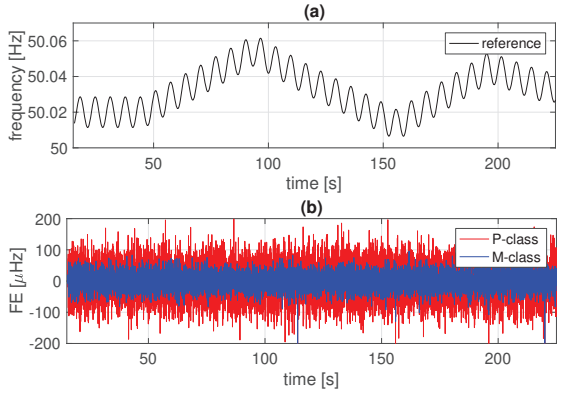

Fig. 4. In (a), the reference value for the fundamental frequency evolution during an inter-area oscillation event. In (b), the FEs obtained by P- and M-class PMU model in red and blue line, respectively.

Then, we described the RTS platform and quantified the models' computational complexity. Finally, we characterized their estimation accuracy in all the IEEE Std tests, as well as in an experimental dataset representative of real-world power system dynamics. In this context, the PMU models prove to be compliant with the requirements of both performance classes (with the only exception of the response time for the P-class *Phase step* test). Based on these results, the developed models might represent a useful tool for investigating the performance of dynamic phasor estimators also in real-world scenarios.

ACKNOWLEDGMENTS

This research project is carried out within the frame of the Swiss Centre for Competence in Energy Research on the Future Swiss Electrical Infrastructure (SCCER-FURIES) with the financial support of the Swiss Innovation Agency.

REFERENCES

[1] I. Kamwa, S. R. Samantaray and G. Joos, *"Compliance Analysis of PMU Algorithms and Devices for Wide-Area Stabilizing Control of Large Power Systems,"* in IEEE Trans. on Pow. Sys., vol. 28, no. 2, pp. 1766-1778, May 2013.

[2] C. Muscas, et al., *"Multiarea Distribution System State Estimation,"* in IEEE Trans. on Instrum. and Meas., vol. 64, no. 5, pp. 1140-1148, May 2015.

[3] *"IEEE Standard for Synchrophasor Measurements for Power Systems,"* in IEEE Std C37.118.1-2011, Dec. 2011.

[4] *"IEEE Standard for Synchrophasor Measurements for Power Systems – Amendment 1: Modification of Selected Performance Requirements,"* in IEEE Std C37.118.1a-2014, April 2014.

[5] D. Ouellette, M. Desjardine, R. Kuffel, Yi Zhang, E. Xu, *"Using a Real Time Digital Simulator with Phasor Measurement Unit technology,"* Int. Conf. on APAP, 2011, vol.3, no., pp.2472,2476, 16-20 Oct. 2011.

[6] D. R. Gurushinghe, A. D. Rajapakse, D. Muthumuni, *"Modeling of a Synchrophasor Measurement Units into an Electromagnetic Transient Simulation Program,"* International Conference on Power Systems Transients (ISPT), Vancouver, Canada July 18-20, 2013.

[7] A. T. Al-Hammouri et al., *"Virtualization of Synchronized Phasor Measurement Units within Real-Time Simulators for Smart Grid Applications,"* IEEE Power and Energy Society General Meeting (PES), 2012, pp.1,7, 22-26 July 2012.

[8] P. Romano, M. Pignati, M. Paolone, *"Integration of an IEEE Std. C37.118 Compliant PMU into a Real-Time Simulator,"* 2015 IEEE Eindhoven PowerTech, Eindhoven, 2015, pp. 1-6.

[9] *"Opal-RT eMEGAsim PowerGrid Real-Time Digital Hardware in the Loop Simulator,"* [online] http://www.opal-rt.com/product/emegasim-powergrid-real-time-digital-hardware-in-the-loop-simulator

[10] M. Bertocco, G. Frigo, C. Narduzzi, C. Muscas and P. A. Pegoraro, *"Compressive Sensing of a Taylor-Fourier Multifrequency Model for Synchrophasor Estimation,"* in IEEE Trans. on Instrum. and Meas., vol. 64, no. 12, pp. 3274-3283, Dec. 2015.

[11] D. Petri, D. Fontanelli and D. Macii, *"A Frequency-Domain Algorithm for Dynamic Synchrophasor and Frequency Estimation,"* in IEEE Trans. on Instrum. and Meas., vol. 63, no. 10, pp. 2330-2340, Oct. 2014.

[12] G. Frigo, A. Derviškadić, Y. Zuo and M. Paolone, *"PMU-Based ROCOF Measurements: Uncertainty Limits and Metrological Significance in Power System Applications"* in IEEE Trans. on Instrum. and Meas., accepted for publication.

[13] A.G. Phadke, J.S. Thorp, *"Synchronized Phasor Measurements and Their Applications,"* Springer, 2017.

[14] J. A. de la O Serna, *"Dynamic Phasor Estimates for Power System Oscillations,"* in IEEE Trans. on Instrum. and Meas., vol. 56, no. 5, pp. 1648-1657, Oct. 2007.

[15] M. A. Platas-Garza, J. A. de la O Serna, *"Dynamic Phasor and Frequency Estimates Through Maximally Flat Differentiators,"* in IEEE Trans. on Instrum. and Meas., vol. 59, no. 7, pp. 1803-1811, July 2010.

[16] P. Castello, M. Lixia, C. Muscas and P. A. Pegoraro, *"Impact of the Model on the Accuracy of Synchrophasor Measurement,"* in IEEE Trans. on Instrum. and Meas., vol. 61, no. 8, pp. 2179-2188, Aug. 2012.

[17] C. Narduzzi, M. Bertocco, G. Frigo and G. Giorgi, *"Fast-TFM—Multifrequency Phasor Measurement for Distribution Networks,"* in IEEE Trans. on Instrum. and Meas., vol. 67, no. 8, pp. 1825-1835, Aug. 2018.

[18] P. Castello, J. Liu, C. Muscas, P. A. Pegoraro, F. Ponci and A. Monti, *"A Fast and Accurate PMU Algorithm for P+M Class Measurement of Synchrophasor and Frequency,"* in IEEE Trans. on Instrum. and Meas., vol. 63, no. 12, pp. 2837-2845, Dec. 2014.

[19] M. Bertocco, G. Frigo, G. Giorgi and C. Narduzzi, *"Frequency Tracking for Efficient Phasor Measurements Based on a CSTFM Model,"* 2015 IEEE AMPS, Aachen, 2015, pp. 1-6.

[20] J. A. de la O Serna and J. Rodriguez-Maldonado, *"Instantaneous Oscillating Phasor Estimates With Taylor^K-Kalman Filters,"* in IEEE Trans. on Pow. Sys., vol. 26, no. 4, pp. 2336-2344, Nov. 2011.

[21] M. Bertocco, G. Frigo, C. Narduzzi and F. Tramarin, *"Resolution Enhancement by Compressive Sensing in Power Quality and Phasor Measurement,"* in IEEE Trans. on Instrum. and Meas., vol. 63, no. 10, pp. 2358-2367, Oct. 2014.

[22] E. Jacobsen and R. Lyons, *"The sliding DFT,"* in IEEE Signal Processing Magazine, vol. 20, no. 2, pp. 74-80, March 2003.

[23] IEEE Interharmonic Task Force, *"Interharmonics in Power Systems,"* Cigre 36.05/CIRED 2 CC02 Voltage Quality Working Group [online] http://grouper.ieee.org/groups/harmonic/iharm/ihfinal.pdf

[24] K. Duda, *"Accurate, Guaranteed Stable, Sliding Discrete Fourier Transform [DSP Tips & Tricks],"* Signal Processing Magazine, IEEE , vol.27, no.6, pp.124-127, Nov. 2010.

[25] P. Romano and M. Paolone, *"An Enhanced Interpolated-Modulated Sliding DFT for High Reporting Rate PMUs,"* 2014 IEEE International Workshop on Applied Measurements for Power Systems Proceedings (AMPS), Aachen, 2014, pp. 1-6.

[26] P. Romano and M. Paolone, *"Enhanced Interpolated-DFT for Synchrophasor Estimation in FPGAs: Theory, Implementation, and Validation of a PMU Prototype,"* in IEEE Trans. on Instrum. and Meas., vol. 63, no. 12, pp. 2824-2836, Dec. 2014.

[27] *"DXE410 PCI Express Expansion Chassis,"* [online] http://www.dolphinics.com/download/DX/OPEN_DOC/DXE410_Product_Brief.pdf

[28] *"Spartan-3 FPGA Family Data Sheet,"* [online] https://www.xilinx.com/support/documentation/data_sheets/ds099.pdf

[29] *"Spectracom PCI Express Slot Cards,"* [online] http://www.spectracomcorp.com/ProductsServices/TimingSynchronization/Bus-level Timing/PCIexpressslotcards/tabid/1296/Default.aspx

[30] G. Frigo, D. Colangelo, A. Derviškadić, M. Pignati, C. Narduzzi and M. Paolone, *"Definition of Accurate Reference Synchrophasors for Static and Dynamic Characterization of PMUs,"* in IEEE Trans. on Instrum. and Meas., vol. 66, no. 9, pp. 2233-2246, Sept. 2017.

[31] P. Castello, C. Muscas, P. Attilio Pegoraro and S. Sulis, *"Critical Analysis of PMU Testing Procedures for Step Response Evaluation,"* 2015 IEEE AMPS, Aachen, 2015, pp. 37-42.